Structure of inhomogeneous Lennard-Jones fluid near the critical region and close to the vapor-liquid coexistence curve: Monte Carlo and density-functional theory studies

Shiqi Zhou
Institute of Modern Statistical Mechanics, Zhuzhou Institute of Technology, Wenhua Road, Zhuzhou city, 412008, People's Republic of China

Andrej Jamnik*
Faculty of Chemistry and Chemical Technology, University of Ljubljana, Aškerčeva 5, SI-1001 Ljubljana, Slovenia
(Received 2 September 2005; revised manuscript received 24 October 2005; published 13 January 2006)

Results for the density profiles of the Lennard-Jones (LJ) fluid subjected to diverse external fields are presented for the Monte Carlo simulations within the grand canonical ensemble and for the third order and second order perturbation density-functional approximation (DFA). In all cases, the bulk LJ fluid in the particle reservoir to which the nonuniform fluid under consideration is connected, is at the conditions situated at "dangerous" regions of the phase diagram, i.e., near the critical temperature or close to the gas-liquid coexistence curve. It is found that the previously investigated third order and second order perturbation DFA for hard core attractive Yukawa fluid [J. Chem. Phys. **122**, 064503 (2005)] can perform successfully also for the nonuniform LJ fluid only on the condition of high accuracy of the required bulk second order direct correlation function. The present report further indicates that the proposed third order and second order perturbation DFA is efficient and suitable for both supercritical and subcritical temperatures.

DOI: 10.1103/PhysRevE.73.011202 PACS number(s): 61.20.−p

I. INTRODUCTION

In recent decades, there has been a considerable interest in research on the structure and thermodynamics of fluids confined in porous materials. Such studies are of substantial importance for the biological and chemical sciences and for related technologies as well. Theoretical studies were usually restricted to idealized physical situations with spherical molecules confined by the smooth solid surfaces. A general feature of the structure of the fluid was its spatial inhomogeneity characterized by a density profile, which was found to display distinct oscillations in the domain close to the walls revealing important packing effects due to the finite size (excluded volume) of the molecules. The period of the oscillations equal to the mean thickness of the layers is, therefore, similar to the molecular diameter. Extensive theoretical work also included computer simulations that confirmed the layering structure of the fluid next to the interfaces.

For the computation of the nonuniform density distribution, a powerful theoretical tool is the classical density-functional theory (DFT). It represents a conventional framework for such structural studies and is important from both, a purely academic point of view as well as from the view of practical applications. Of course, one requires a high accuracy of the DFT predictions and simultaneously its applicability to both supercritical and subcritical temperature regimes. However, the majority of the existing density-functional approximations (DFA) do not comprise these two advantages at the same time. An exception represents a recently proposed partitioned DFA [1], that treats the tail part of the correlation function by employing the second order functional perturbative expansion approximation (FPEA), while its hard-core part is treated by utilizing directly a Lagrangian theorem-based hard-sphere DFA. Here the term "directly" denotes a direct substitution of the hard-sphere correlation functions in the Lagrangian theorem-based hard-sphere DFA by the hard-core part of the non-hard-sphere fluid correlation functions. The Lagrangian theorem-based hard-sphere DFA requires the direct correlation functions (DCF) for different bulk densities as inputs. The problem is that there is no numerical solution for the second order DCFs when the model parameters of the equilibrium bulk fluid are situated within the gas-liquid coexistence region. For this reason, the resultant partitioned DFA breaks down for the bulk phase coexistence regime, even in the case when it should possess high accuracy due to incorporation of an adjustable parameter. One of the fundamental ways of solving this awkward situation is to employ a hard-sphere DFA, which in contrast to the Lagrangian theorem-based or other hard-sphere DFAs, requires only the DCF for a single coexistence bulk density as an input. One example of such hard-sphere DFAs is the hard-sphere third order FPEA based on an approximate analytical expression for the bulk third order DCF [2], the resultant DFA being called the third order and second order perturbation DFT approach. Its performance for the nonuniform hard-core attractive Yukawa (HCAY) model fluid subjected to diverse external fields was investigated in detail in our previous work [3]. On the basis of a comparison between the theoretical predictions and simulation data we found that the third order and second order perturbation DFT approach could capture the physics of the nonuniform HCAY model fluid only in the case of high reliability of the imported bulk second order DCF. Therein, the latter function

*Email address: andrej.jamnik@fkkt.uni-lj.si

was based on the Ornstein-Zernike (OZ) integral equation supplemented by the mean spherical approximation (MSA) for the HCAY fluid [4]. The quality of the performance of the perturbation DFT approach was found to be sensitive to the values of bulk model parameters stemming from the dependence of the accuracy of the MSA bulk second order DCF on the bulk density and potential parameters. Accordingly, the reliability of the perturbation DFT approach was found to conform to the accuracy of the externally imported bulk second order DCF. The high accuracy of the latter is thus of crucial importance for the successful performance of the third order and second order perturbation DFT.

In the present work we explore the structural properties of the Lennard-Jones fluid, which is a prototype model for realistic intermolecular interactions. The LJ model is especially popular also as a sample model used for critical tests of statistical mechanical theories. It has received much attention for years and numerous studies of such systems have been continuously emerging in the literature. A series of theoretical studies appeared in a very recent investigation dealing with both the pure LJ fluid and LJ mixtures in bulk [5,6] or in confined systems [7]. By a suitable adjustment of the potential parameters it has been employed to describe the phase behavior [5] and interfacial properties [6] of various real systems. Further, it has proven to be useful in the description of various properties and phenomena that take place at solid-fluid interfaces and in pores [7], e.g., adsorption, interfacial tension, and wetting.

The first aim of this investigation is to propose the simulation data for the LJ fluid subjected to different external fields. The inhomogeneous LJ fluid maintains the equilibrium with the bulk phase at the conditions referring either to the supercritical states located close to the critical region or to the subcritical states located in the vicinity of the gas-liquid coexistence curve. The resulting simulation data then offer a strict test for the accuracy of the present third order and second order perturbation DFT approach as well as for any future's DFAs. A second purpose of the present work is to apply the third order and second order perturbation DFT approach to nonuniform LJ fluid by employing an accurate numerical solution for the bulk LJ second order DCF as an input. According to the conclusions following from the analysis of the results for inhomogeneous HCAY fluid gathered in Ref. [3], the resultant DFA for the nonuniform LJ fluid is expected to be reliable due to the high accuracy of the imported bulk second order DCF. Such features regarding the quality of the performance of the present DFA would serve as additional firm evidence of the conclusions summarized in Ref. [3].

The details of the model and simulation are described in Sec. II. In Sec. III, a description of the present third order and second order perturbation DFT approach for the LJ fluid is given. Numerical results for a variety of situations are collected and the performance of the DFT approach is evaluated. Finally, some concluding remarks are summarized in Sec. IV.

II. SIMULATION METHOD

In this work, as a target model, we employ the Lennard-Jones potential function, which incorporates the essential features of real molecules. It is given by

$$u_{lj}(r) = 4\varepsilon\left[\left(\frac{r}{\sigma}\right)^{-12} - \left(\frac{r}{\sigma}\right)^{-6}\right], \tag{1}$$

where ε and σ establish the energy and length scales of the potential. In the following the reduced units are used for the absolute temperature T, $T^*=kT/\varepsilon$ with k being the Boltzmann constant.

For the LJ model of Eq. (1) we have carried out grand canonical ensemble Monte Carlo (GCEMC) simulations at a constant chemical potential μ, volume V, and temperature T. This set of independent parameters that define the thermodynamic state of the system made possible the study of equilibrium between the bulk LJ fluid and that subjected to various external fields originating from the presence of various spatial constrains. For the latter, we have chosen in turn a hard flat interface, a planar slit consisting of two parallel, perfectly smooth hard walls, a closed spherical surface mimicking a spherical cavity, and finally, a single large hard sphere. The general features of the GCEMC method are described elsewhere [8]. Further, some details peculiar to this study are discussed in our previous work and we refer the reader to Ref. [3]. The liquid-gas phase behavior of the pure LJ fluid was investigated by Potoff and Panagiotopoulos [9]. By using grand canonical Monte Carlo simulations they determined the liquid-vapor coexistence curve and critical point. The critical parameters of the untruncated LJ potential were assessed as $T_c^*=1.312$ and $\rho_c^*=0.316$. We have performed calculations for three sets of reduced temperatures, the value of the first set being slightly higher, and those of the latter two sets slightly lower or well below the critical value 1.312. The ratio between the chosen supercritical temperature and the critical value was approximately 1.008. For this regime, a broad range of bulk reduced densities ranging from the value 0.1 to 0.8 has been investigated. The ratios between the chosen subcritical temperatures and the critical value were approximately 0.65 and 0.8, respectively. For the subcritical regimes, however, only narrow 1-phase regions corresponding either to monophasic gaseous state (low densities) or monophasic liquid states (high densities) could be explored. For this reason, there are only a few simulation data presented for these regimes.

III. THIRD AND SECOND ORDER PERTURBATIVE DFT

First, in summary we recapitulate the third order and second order perturbation DFT approach [3,10]. The approximate analytical expression for the bulk third order DCF of the hard-sphere (HS) fluid is given by [2]

$$C_{0hs}^{(3)}(\mathbf{r},\mathbf{r}_1,\mathbf{r}_2;\rho_b) = \frac{C_{0hs}^{(1)^2}(\rho_b)}{[C_{0hs}^{(1)'}(\rho_b)]^3}\int C_{0hs}^{(2)}(\mathbf{r}_0,\mathbf{r};\rho_b)C_{0hs}^{(2)}(\mathbf{r}_0,\mathbf{r}_1;\rho_b) \times C_{0hs}^{(2)}(\mathbf{r}_0,\mathbf{r}_2;\rho_b)d\mathbf{r}_0, \tag{2}$$

where the subscript "hs" denotes the quantities for the HS fluid. Throughout the text, superscript (n) denotes the corresponding n-order quantities; absence of the subscript 0 refers to the nonuniform case, while the presence of the subscript 0 refers to the uniform case.

Functional perturbation expansion of the nonuniform first order DCF $C_{hs}^{(1)}(\mathbf{r};[\rho])$ for HS fluid around the equilibrium bulk density ρ_b leads to the expression

$$C_{hs}^{(1)}(\mathbf{r};[\rho]) = C_{0hs}^{(1)}(\rho_b) + \int d\mathbf{r}_1[\rho(\mathbf{r}_1)-\rho_b]C_{0hs}^{(2)}(|\mathbf{r}-\mathbf{r}_1|;\rho_b) + \sum_{n=3}^{\infty}\frac{1}{(n-1)!}\int d\mathbf{r}_1\int d\mathbf{r}_2,\ldots,\int d\mathbf{r}_{n-1} \times\prod_{m=1}^{n-1}[\rho(\mathbf{r}_m)-\rho_b]C_{0hs}^{(n)}(\mathbf{r},\mathbf{r}_1,\ldots,\mathbf{r}_{n-1};\rho_b). \quad (3)$$

Discarding away all of the terms with $n>3$ in the sum of Eq. (3) then yields

$$C_{hs}^{(1)}(\mathbf{r};[\rho]) = C_{0hs}^{(1)}(\rho_b) + \int d\mathbf{r}_1[\rho(\mathbf{r}_1)-\rho_b]C_{0hs}^{(2)}(|\mathbf{r}-\mathbf{r}_1|;\rho_b) + \frac{1}{2}\int d\mathbf{r}_1\int d\mathbf{r}_2\prod_{m=1}^{2}[\rho(\mathbf{r}_m)-\rho_b] \times C_{0hs}^{(3)}(\mathbf{r},\mathbf{r}_1,\mathbf{r}_2;\rho_b). \quad (4)$$

A combination of Eqs. (2) and (4) leads to the so-called hard-sphere third order perturbation DFT approach,

$$C_{hs}^{(1)}(\mathbf{r};[\rho]) = C_{0hs}^{(1)}(\rho_b) + \int d\mathbf{r}'[\rho(\mathbf{r}')-\rho_b]C_{0hs}^{(2)}(|\mathbf{r}-\mathbf{r}'|;\rho_b) + \frac{C_{0hs}^{(1)''}(\rho_b)}{2[C_{0hs}^{(1)'}(\rho_b)]^3}\int C_{0hs}^{(2)}(\mathbf{r},\mathbf{r}'';\rho_b) \times\left\{\int C_{0hs}^{(2)}(\mathbf{r}',\mathbf{r}'';\rho_b)[\rho(\mathbf{r}')-\rho_b]d\mathbf{r}'\right\}^2 d\mathbf{r}''; \quad (5)$$

where a prime and a double prime denote first and second order density derivatives, respectively.

In the framework of the partitioned DFT formalism [1] one splits the bulk second order DCF $C_0^{(2)}(r;\rho_b,\ldots)$ into the hard-core part $C_{0hc}^{(2)}(r;\rho_b,\ldots)$ and tail part $C_{0tail}^{(2)}(r;\rho_b,\ldots)$:

$$C_0^{(2)}(r;\rho_b,\ldots) = C_{0hc}^{(2)}(r;\rho_b,\ldots) + C_{0\ tail}^{(2)}(r;\rho_b,\ldots), \quad (6)$$

where

$$C_{0hc}^{(2)}(r;\rho_b,\ldots) = C_0^{(2)}(r;\rho_b,\ldots) \quad r<r_{cut}; \qquad =0 \quad r>r_{cut} \quad (7)$$

and

$$C_{0\ tail}^{(2)}(r;\rho_b,\ldots) = 0 \quad r<r_{cut}; \qquad = C_0^{(2)}(r;\rho_b\ldots) \quad r>r_{cut}. \quad (8)$$

Further, we have similarly

$$C^{(1)}(\mathbf{r};[\rho],\ldots) = C_{hc}^{(1)}(\mathbf{r};[\rho],\ldots) + C_{tail}^{(1)}(\mathbf{r};[\rho],\ldots) \quad (9)$$

and

$$C_0^{(1)}(\rho_b,\ldots) = C_{0hc}^{(1)}(\rho_b,\ldots) + C_{0\ tail}^{(1)}(\rho_b,\ldots). \quad (10)$$

Here, the set $\rho_b,\ldots$ stands for the bulk density and potential parameters. The tail part $C_{0tail}^{(2)}(r;\rho_b,\ldots)$ is usually only weakly dependent on the density argument [1]. This allows the tail part $C_{tail}^{(1)}(\mathbf{r};\rho_b,\ldots)$ of the nonuniform first order DCF to be treated by the second order functional perturbation expansion approximation (FPEA) [1]

$$C_{tail}^{(1)}(\mathbf{r};[\rho],\ldots) = C_{0\ tail}^{(1)}(\rho_b,\ldots) + \int d\mathbf{r}_1[\rho(\mathbf{r}_1)-\rho_b]C_{0\ tail}^{(2)}(|\mathbf{r}-\mathbf{r}_1|;\rho_b,\ldots). \quad (11)$$

For the hard-core part, one can directly apply the so-called hard-sphere third order perturbation DFT approach comprised in Eq. (5). Here, the term "directly" means a direct substitution of the quantities for the HS fluid by the corresponding quantities for hard-core parts in the hard-sphere third order perturbation DFT approach. After applying directly Eq. (5) the to hard-core part, one has

$$C_{hc}^{(1)}(\mathbf{r};[\rho],\ldots) = C_{0hc}^{(1)}(\rho_b,\ldots) + \int d\mathbf{r}'[\rho(\mathbf{r}')-\rho_b]C_{0hc}^{(2)}(|\mathbf{r}-\mathbf{r}'|;\rho_b,\ldots) + \frac{C_{0hc}^{(1)''}(\rho_b,\ldots)}{2[C_{0hc}^{(1)'}(\rho_b,\ldots)]^3}\int C_{0hc}^{(2)}(\mathbf{r},\mathbf{r}'';\rho_b,\ldots) \times\left\{\int C_{0hc}^{(2)}(\mathbf{r}',\mathbf{r}'';\rho_b,\ldots)[\rho(\mathbf{r}')-\rho_b]d\mathbf{r}'\right\}^2 d\mathbf{r}''. \quad (12)$$

Further, a combination of Eqs. (6)–(12) leads to

$$C^{(1)}(\mathbf{r};[\rho],\ldots) = C_0^{(1)}(\rho_b,\ldots) + \int d\mathbf{r}'[\rho(\mathbf{r}')-\rho_b]C_{0hc}^{(2)}(|\mathbf{r}-\mathbf{r}'|;\rho_b,\ldots) + \frac{C_{0hc}^{(1)''}(\rho_b,\ldots)}{2[C_{0hc}^{(1)'}(\rho_b,\ldots)]^3}\int C_{0hc}^{(2)}(\mathbf{r},\mathbf{r}'';\rho_b,\ldots) \times\left\{\int C_{0hc}^{(2)}(\mathbf{r}',\mathbf{r}'';\rho_b,\ldots)[\rho(\mathbf{r}')-\rho_b]d\mathbf{r}'\right\}^2 d\mathbf{r}'' + \int d\mathbf{r}_1[\rho(\mathbf{r}_1)-\rho_b]C_{0\ tail}^{(2)}(|\mathbf{r}-\mathbf{r}_1|;\rho_b,\ldots) = C_0^{(1)}(\rho_b,\ldots) + \int d\mathbf{r}'[\rho(\mathbf{r}')-\rho_b]C_0^{(2)}(|\mathbf{r}-\mathbf{r}'|;\rho_b,\ldots) + \frac{C_{0hc}^{(1)''}(\rho_b,\ldots)}{2[C_{0hc}^{(1)'}(\rho_b,\ldots)]^3}\int C_{0hc}^{(2)}(\mathbf{r},\mathbf{r}'';\rho_b,\ldots)$$

$$\times\left\{\int C_{0hc}^{(2)}(\mathbf{r}',\mathbf{r}'';\rho_b,\ldots)[\rho(\mathbf{r}')-\rho_b]d\mathbf{r}'\right\}^2 d\mathbf{r}''. \tag{13}$$

The coefficient

$$\frac{C_{0hc}^{(1)''}(\rho_b,\ldots)}{2[C_{0hc}^{(1)'}(\rho_b,\ldots)]^3}$$

in the last Eq. (13) is used as an adjustable parameter denoted by λ. Then we finally have

$$\begin{aligned}C^{(1)}(\mathbf{r};[\rho],\ldots)=C_0^{(1)}(\rho_b,\ldots)+\int d\mathbf{r}'[\rho(\mathbf{r}')-\rho_b]C_0^{(2)}(|\mathbf{r}\\ -\mathbf{r}'|;\rho_b,\ldots)+\lambda(\rho_b,\ldots)\int C_{0hc}^{(2)}\\ \times(\mathbf{r},\mathbf{r}'';\rho_b,\ldots)\left\{\int C_{0hc}^{(2)}(\mathbf{r}',\mathbf{r}'';\rho_b,\ldots)\right.\\ \left.\times[\rho(\mathbf{r}')-\rho_b]d\mathbf{r}'\right\}^2 d\mathbf{r}''.\end{aligned} \tag{14}$$

In our previous works [3,10], Eq. (14) was combined with the single component density profile given by

$$\rho(\mathbf{r})=\rho_b\exp\{-\beta\varphi_{ext}(\mathbf{r})+C^{(1)}(\mathbf{r};[\rho],\ldots)-C_0^{(1)}(\rho_b,\ldots)\} \tag{15}$$

used to predict the structure of the HCAY fluid subjected to diverse external fields. Here $\varphi_{ext}(\mathbf{r})$ is the external potential responsible for the generation of the inhomogeneous spatial density distribution $\rho(\mathbf{r})$, and β is the inverse thermal energy, $\beta=1/kT$, k being the Boltzmann constant and T the absolute temperature. In the present work Eqs. (14) and (15) are applied for the calculation of the density profiles of the LJ fluid under the influence of different external fields.

The LJ potential $u_{lj}(r)$ is truncated and shifted at r_c, the resultant potential $u_{lj}^{ts}(r)$ is given by

$$\begin{aligned}u_{lj}^{ts}(r)&=u_{lj}(r)-u_{lj}(r_c), \quad r\leqslant r_c\\ &=0, \qquad\qquad\quad r\geqslant r_c.\end{aligned} \tag{16}$$

The required bulk second order DCF $C_0^{(2)}(r;\rho_b,\ldots)$ is obtained numerically from the OZ integral equation

$$\begin{aligned}\gamma(r)&=h(r)-C_0^{(2)}(r;\rho_b,\ldots)\\ &=\rho_b\int d\mathbf{r}_1 h(\mathbf{r}_1)C_0^{(2)}(|\mathbf{r}-\mathbf{r}_1|;\rho_b,\ldots)\end{aligned} \tag{17}$$

along with the closure relation

$$h(r)+1=\exp\{-u_{lj}^{ts}(r)+\gamma+B(s)\}. \tag{18}$$

Above, $\gamma(r)$ is the indirect correlation function, $s=\gamma(r)-\beta u_2(r)$ is the so-called renormalization indirect correlation function, $h(r)=g(r)-1$ is the total correlation function with $g(r)$ the radial distribution function, and B is the bridge functional specified as follows:

$$\begin{aligned}B(s)&=\frac{-s^2}{2[1+0.8s]}, \quad s\geqslant 0\\ &=-0.5s^2, \qquad\quad s<0.\end{aligned} \tag{19}$$

The bridge functional Eq. (19) is obtained by substituting a well-known Verlet-modified (VM) bridge functional with $-0.5s^2$ for $s<0$ [11], and leaving the VM bridge functional unchanged for $s\geqslant 0$. In spite of the fact that there exist other more developed bridge function approximations, e.g., those proposed by Choudhury and Ghosh [12] and by Bomont and Bretonnet [13], we have still chosen the more simple bridge function approximation given by Eq. (19) for the following reasons. When we consider the properties of more complex fluids, e.g., the effective interactions between the large solute particles immersed in a molecular solvent, the effective potential between the solute particles is affected by both the properties of the solvent and those due to the solvent-solute interactions. For the former case of the simple atomic fluids there exist, of course, various potentials for the description of the interparticle interactions. Since it is impossible to propose the bridge function approximation for each of the individual potentials, it is desirable to keep a simple and general method for the determination of the bridge function for all of these potentials consisting of the hard-core repulsion and long range attractive (tail) interactions. The resulting bulk second order DCF is then sufficient as an input for the present third order and second order perturbation DFT approach. Why have we chosen exactly the mathematical form of Eq. (19)? First, this choice is based on the observation that the VM bridge function has been tested repeatedly and positively. The next reason stems from the fact that its single point in region $s<0$ leads to a divergence of the numerical solution, and the term $-0.5s^2$ is exactly the leading term in the Taylor series expansion of many bridge function approximations such as Percus-Yevick (PY), Martynov-Sarkisov (MS), and the VM approximation [14]. In fact, the calculations presented in this work enable one to be convinced that the bulk second order DCF resulting from the present general specification of the bridge function, Eq. (19), is sufficient as an input for the present DFT approach. The expression for the perturbation part of the potential $\beta u_2(r)$ is taken from the Ref. [15]. The adjustable parameter λ we determine by a single hard wall sum rule, similarly as done in our previous works on HCAY fluid [3,10].

As the HCAY model includes a hard-sphere repulsion in the interparticle potential of the interaction, it was natural to set the value for r_{cut} equal to the diameter of hard sphere. On the contrary, the LJ potential includes strong soft-core repulsion instead of a pure hard-sphere repulsive core, thus giving

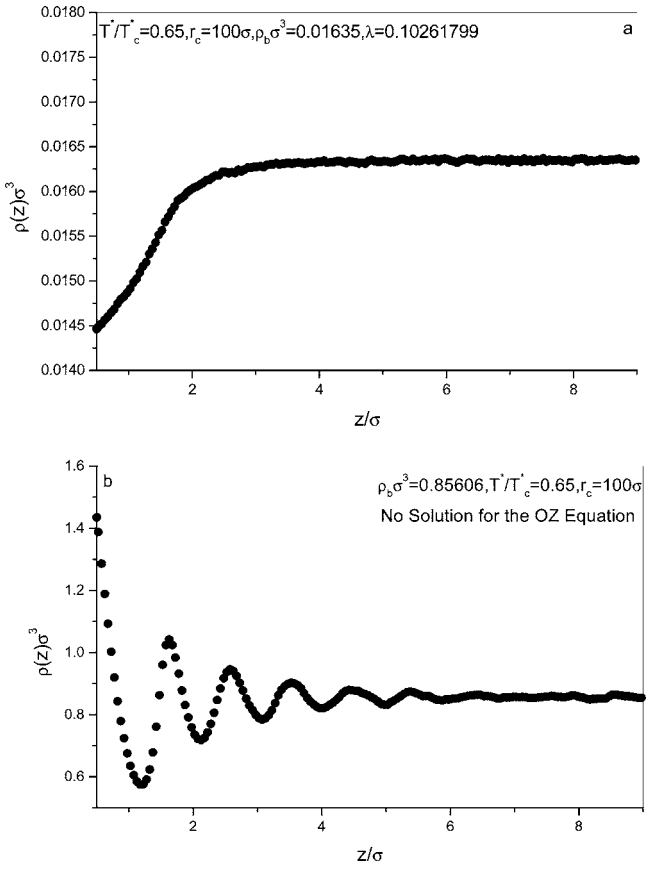

FIG. 1. The theoretical (lines) and simulation (symbols) results for the density profiles of the LJ fluid near a single hard wall at the ratio between the actual and critical reduced temperature T^*/T_c^* =0.65 and at different values of the bulk reduced density.

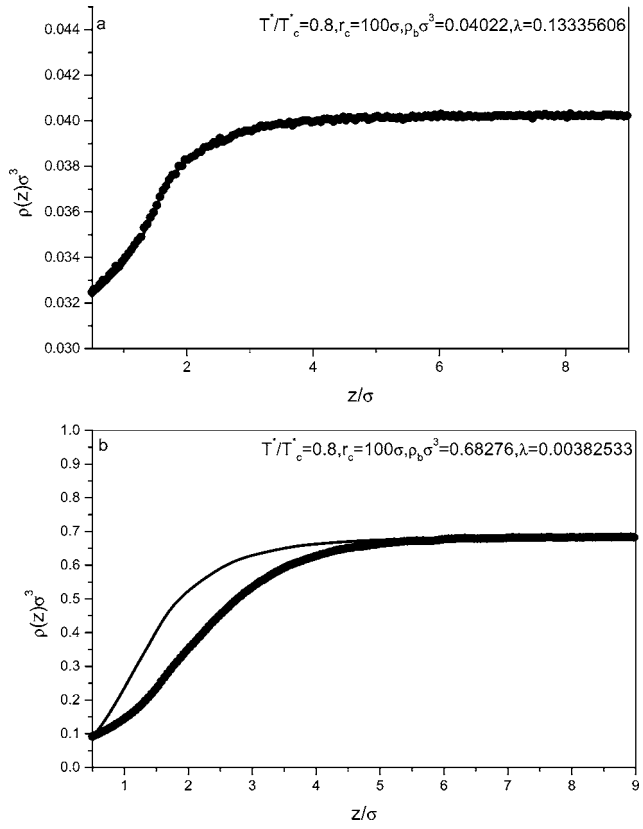

FIG. 2. Same as Fig. 1 but for $T^*/T_c^*=0.8$.

rise to its more elusive treatment (perplexed by a problem of specifying the equivalent hard-core diameter) than in the case of other models comprising a hard-sphere core in the pair interaction potential. For this reason, the LJ model serves as an even stricter sample potential for testing the DFA theory than other models.

We investigate several cases of the source for the external potential. Besides the single hard wall, we treat also a planar gap, i.e., the two hard walls separated by a distance H, a spherical cavity surrounded by a spherical hard wall, a large hard spherical particle, and a bulk LJ particle. The external potentials due to the presence of these spatial constrains read in turn

$$\begin{aligned} \varphi_{ext}(z) &= \propto \quad z/\sigma < 0.5 \\ &= 0 \quad 0.5 < z/\sigma \end{aligned} \tag{20}$$

for a single hard wall,

$$\begin{aligned} \varphi_{ext}(z) &= \propto \quad z/\sigma < 0.5 \text{ or } z/\sigma > H/\sigma - 0.5 \\ &= 0 \qquad 0.5 < z/\sigma < H/\sigma - 0.5 \end{aligned} \tag{21}$$

for a planar slit with two plane hard walls situated at $z=0$ and $z=H$, respectively,

$$\begin{aligned} \varphi_{ext}(\mathbf{r}) &= \propto \quad |\mathbf{r}/\sigma| < R/\sigma \\ &= 0 \quad |\mathbf{r}/\sigma| > R/\sigma \end{aligned} \tag{22}$$

for a large hard spherical particle,

$$\begin{aligned} \varphi_{ext}(\mathbf{r}) &= \propto \quad |\mathbf{r}/\sigma| > R/\sigma \\ &= 0 \quad |\mathbf{r}/\sigma| < R/\sigma \end{aligned} \tag{23}$$

for a spherical cavity with hard spherical wall of effective radius R, and

$$\varphi_{ext}(\mathbf{r}) = u_{lj}^{ts}(r) \tag{24}$$

for a bulk LJ particle. For the latter case Eq. (24), the reduced density distribution function $\rho(\mathbf{r})/\rho_b$ is actually the bulk RDF $g(\mathbf{r})$ according to the Percus's test particle method [16].

First, the adjustable parameter λ for each set of parameters of the coexistence bulk fluid is determined by the single hard wall sum rule. The pressure of the equilibrium bulk fluid required for this purpose is obtained by considering the contact theorem relating the pressure and the contact density. For the latter we employ the exact simulation result, the pressure being equal to $\rho(0.5\sigma)/\beta$. It means that the parameter λ is adjusted to the value ensuring the equality of the contact density predicted by the present DFT approach and that obtained by the "exact" simulation method.

The density profiles of the LJ fluid subjected to diverse external fields at the supercritical temperature $1.008T_c^*$ and at two subcritical temperatures $0.65T_c^*$ and $0.80T_c^*$, respectively,

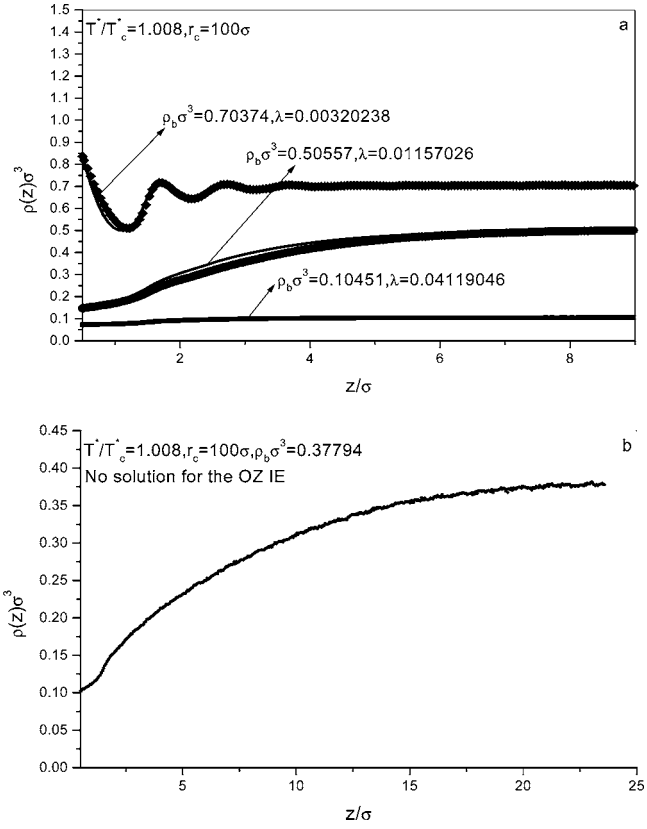

FIG. 3. Same as Fig. 1 but for $T^*/T_c^*=1.008$.

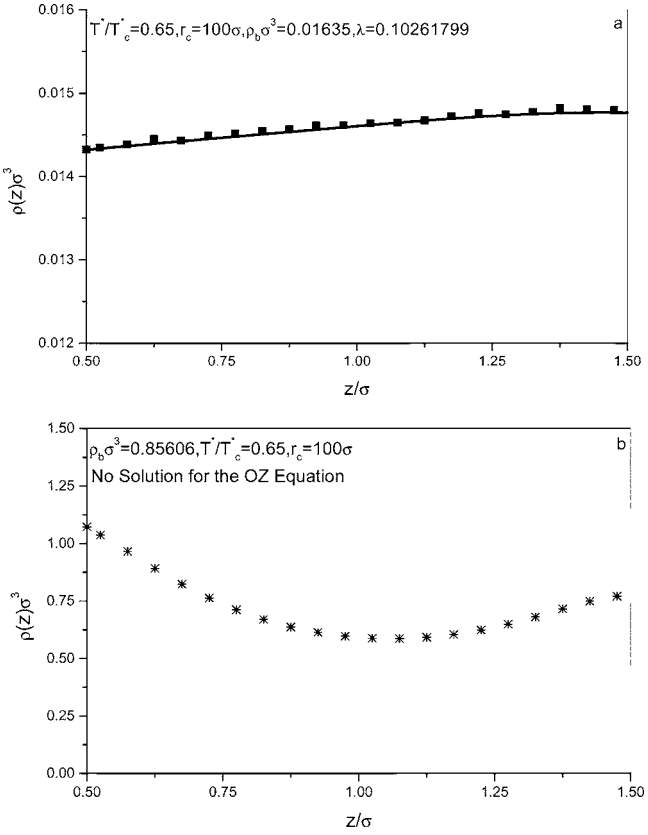

FIG. 4. The theoretical (lines) and simulation (symbols) results for the single wall density profiles of the LJ fluid in the planar gap of width $H=3\sigma$ at the ratio between the actual and critical reduced temperature $T^*/T_c^*=0.65$ and at different values of the bulk reduced density.

are presented in Figs. 1–14. For the supercritical regime, the values of the bulk reduced density cover a broad range from 0.1 to 0.8. Subcritical regime, however, is represented by only a few values of the bulk density lying in narrow 1-phase regions of the phase diagram corresponding either to a monophasic gaseous state (low densities) or a monophasic liquid state (high densities). In turn, the figures show the density profiles of the LJ fluid: (i) at a single hard wall (Figs. 1–3), (ii) in the planar gap of width $H=3\sigma$ (Figs. 4–6), (iii) near a large hard sphere of effective radius $R=5.5\sigma$ (Fig. 7–9), (iv) in a hard spherical cavity of effective radius $R=3.5\sigma$ (Figs. 10–12), and (v) the radial distribution function of the bulk LJ fluid (Figs. 13 and 14). In all cases the corresponding values for the adjustable parameter λ, obtained for each temperature and bulk density, are also presented. For the sake of clarity, the majority of figures are subdivided into two parts, where the separate parts contain the results for the same set of the model parameters except the bulk densities.

As can be noticed in Figs. 1(b), 3(b), 4(b), 6(a), 7(b), 10(b), 12(a), 13(a), and 14, the DFT results for the density profiles or reduced density profiles are missing when the coexistence bulk fluid is at the conditions corresponding to the following parameter combinations: (i) $\rho_b\sigma^3=0.37794$, $T^*/T_c^*=1.008$ (in the phase diagram, this supercritical state is located close to the critical point) and (ii) $\rho_b\sigma^3=0.85606$, $T^*/T_c^*=0.65$ (this subcritical state is located in the vicinity of the gas-liquid coexistence curve). This lack of the theoretical data stems from the fact that there are no numerical solutions to the OZ equation for these two sets of parameters even though the simulation results indicate the thermodynamic stability of these states. This deficiency, however, is not caused by the theory itself, but due to the unavailability of the exact bridge function. The predictions for the phase diagram following from any bridge function approximation including the more developed ones, e.g., those proposed by Choudhury and Ghosh [12] and by Bomont and Bretonnet [13], certainly do not coincide completely with the phase diagram being intrinsically associated with the potential function. Accordingly, some small deviations between the theoretical and the "true" (referring to simulation) phase diagram always exist. It is therefore possible that some thermodynamically stable states referring to the simulation data fall into the gas-liquid coexistence region of the phase diagram resulting from the pure theory. Consequently, the OZ integral equation provides nonphysical results in such cases.

A careful inspection of the presented local structures of the LJ fluid near the hard obstacles or in confined systems leads to a conclusion that the quality of the performance of the DFT theory depends on the expressiveness of the "inhomogeneity" of the system. For this reason, the theory does the best job in the homogeneous case of the bulk fluid (Figs. 13 and 14), whereas the most pronounced discrepancies between the theoretical predictions and the simulation data can be observed in the case of the highest degree of confinement imposed by the presence of the spherical wall (Figs. 10–12). A fair to excellent agreement between the DFT and GCEMC

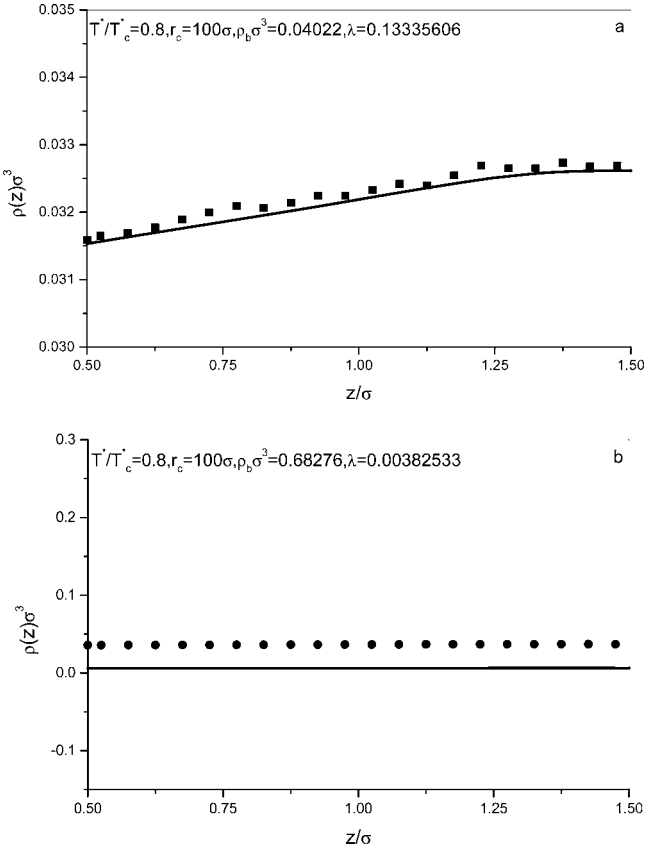

FIG. 5. Same as Fig. 4 but for $T^*/T_c^*=0.8$.

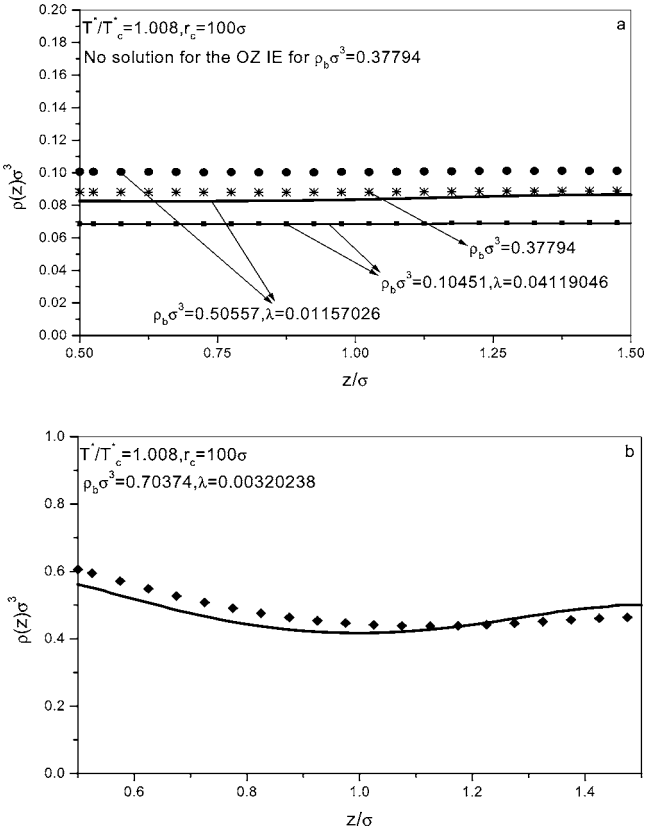

FIG. 6. Same as Fig. 4 but for $T^*/T_c^*=1.008$.

density profiles near a single hard wall seen in Figs. 1–3 stem also from the fact that the adjustable parameter λ is determined by the single hard wall sum rule, where this parameter is adjusted to the value ensuring the equality of the DFT and GCEMC contact densities.

For subcritical temperatures $T^*/T_c^*=0.65$ and 0.8, and low bulk density (gaseous state in the phase diagram of the bulk fluid) the theory performs excellently in the case of a single wall [Figs. 1(a) and 2(a)], the same being true also in the case of a large hard sphere as a source of an external field [Figs. 7(a) and 8(a)]. The agreement between the results for the structure of the fluid in a planar gap [Figs. 4(a) and 5(a)] and in a spherical cavity [Figs. 10(a) and 11(a)] obtained by both methods is slightly worsened in comparison to that for a single wall, although the theoretical results still agree qualitatively with the simulation data. As expected, this disagreement is somewhat more pronounced in the latter case of a spherical cavity as it represents the most restricted geometry of the system. For $T^*/T_c^*=0.8$, where we dispose of the theoretical data also for the higher bulk density (the liquid state in the phase diagram of the bulk fluid), the DFT predictions deviate from the simulation data in all cases of the external potentials [Figs. 2(b), 5(b), 8(b), and 11(b)]. The large deviation for these subcritical, high density cases is ascribed to drying transition. As shown in Figs. 2(b), 5(b), 8(b), and 11(b), magnitude of the density profile is far lower than the corresponding coexistence bulk density. It is exactly the large difference between the density profile and the coexistence bulk density that leads to the worsened performance. In fact, all of existing DFT approaches [17] are associated with this point. In Ref. [17], the predicted drying transition point deviates so from the simulational one that the percent relative error is high up to 60. From Figs. 2(b), 5(b), 8(b), and 11(b), one can judge that the present deviation, although obvious, is absolutely not so large as in the case in Ref. [17]. The worsened performance of the presently existing DFT approaches for a drying transition is due to the expression appearing

in the density profile equation: $\int d\mathbf{r}'[\rho(\mathbf{r}')-\rho_b]C_{0tail}^{(2)}(|\mathbf{r}-\mathbf{r}'|;\rho_b,\ldots)$ for the present case, and $-\int d\mathbf{r}'[\rho(\mathbf{r}')-\rho_b]\beta u_{attr}(|\mathbf{r}-\mathbf{r}'|)$ (u_{attr} is the attractive part of the interaction potential) for the case in Ref. [17]; these two expressions result, respectively, from truncating a series expansion and a mean field approximation which is also associated with discarding away higher terms; a large difference $\rho(\mathbf{r}')-\rho_b$ leads also to large omitted higher terms.

On the contrary, the DFT structure of the bulk fluid for the same set of parameters still coincides perfectly with the simulation results [Fig. 13(b)]. A similar judgment about the performance of the present DFT approach in predicting the structure of the fluid subjected to various external potentials can be drawn also from the results referring to the supercritical temperature $T^*/T_c^*=1.008$ (Figs. 3, 6, 9, and 12). Again the theory performs well for a single hard wall (Fig. 3) and for a large hard sphere (Fig. 9) as spatial constraints, and somewhat worse for the confined systems of a planar gap (Fig. 6) and a spherical cavity (Fig. 12). In the latter cases it is interesting to observe the extent of the deviations of the

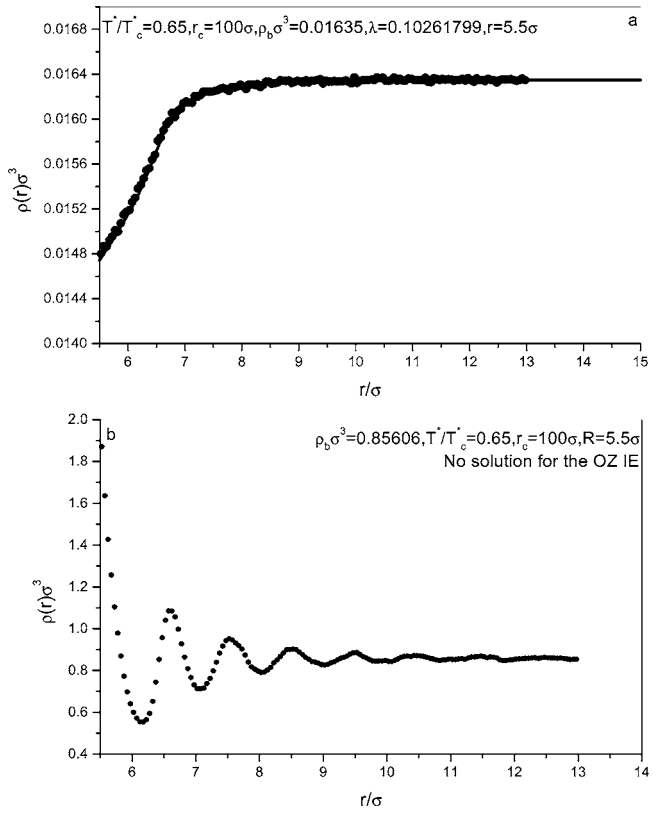

FIG. 7. The theoretical (lines) and simulation (symbols) results for the density profiles of the LJ fluid near a large spherical particle of an effective radius $R=5.5\sigma$ at the ratio between the actual and critical reduced temperature $T^*/T_c^*=0.65$ and at different values of the bulk reduced density.

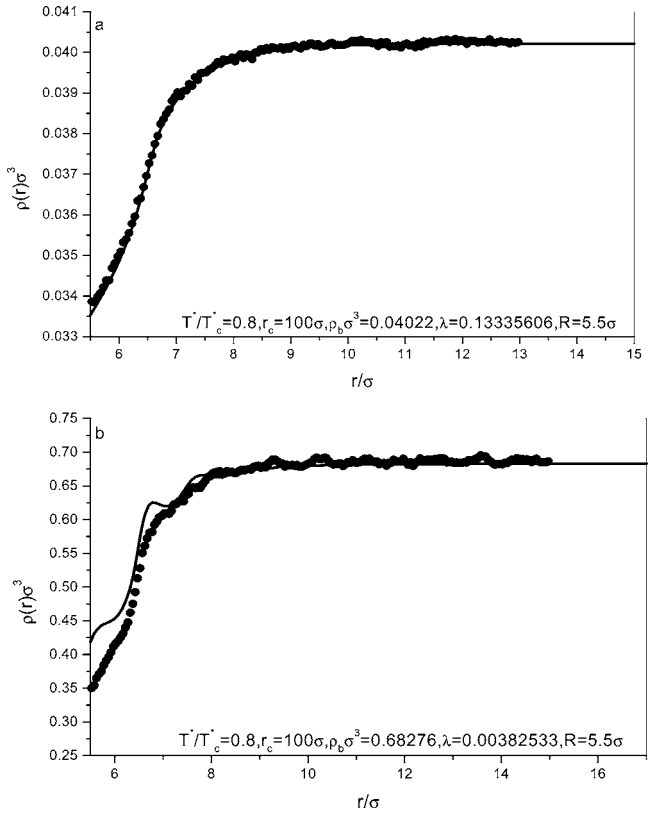

FIG. 8. Same as Fig. 7 but for $T^*/T_c^*=0.8$.

DFT results from the GCEMC data at different bulk densities. As seen from Figs. 6 and 12, these deviations are the most appreciable at the intermediate bulk density (approx. 0.5) and somewhat less pronounced at higher and lower densities (approx. 0.7 and 0.1, respectively). This feature stems from the fact that the intermediate density corresponds to the condition of the bulk fluid lying in the most vicinity to the critical point.

A global observation following from the comparison between the theoretical predictions and simulation data leads to a conclusion that although the RDF of the bulk LJ fluid can be predicted very accurately by the proposed third order and second order perturbation DFT approach, the results for the various confined geometries are somewhat worse. Clearly, the bulk RDF originates from an external field caused by a bulk LJ particle, which exerts an external potential consisting of a soft repulsion plus an attractive tail interaction on the fluid particles. This is exactly the reason for our choice of the hard external potentials to test the performance of the proposed DFA approach. At a given set of bulk density and potential parameters, the value of the adjustable parameter λ is determined by a single hard wall sum rule, the same value of this parameter is then used in the case of other external potentials. This embodies the universality of the adjustable parameter λ, i.e., its independence on the particular external field responsible for the generation of the spatial inhomogeneous structure of the fluid. In our previous papers [3,10], we employed the MSA/OZ solution for the required bulk second order DCF for the HCAY fluid. As the accuracy of this function changed upon changing the bulk density and potential parameters, the same was true for the performance of the resultant DFA. On the contrary, the bulk second order DCF applied in this study is obtained by the numerical solution of the OZ integral equation, which is generally more accurate than the MSA solution for the HCAY model. Consequently, the resultant accuracy of the predictions for the density profiles in the present theoretical study is generally improved in comparison with the previous case of MSA-based second order DCF for the HCAY fluid. This fact further illustrates that the present third order and second order DFA is struc-

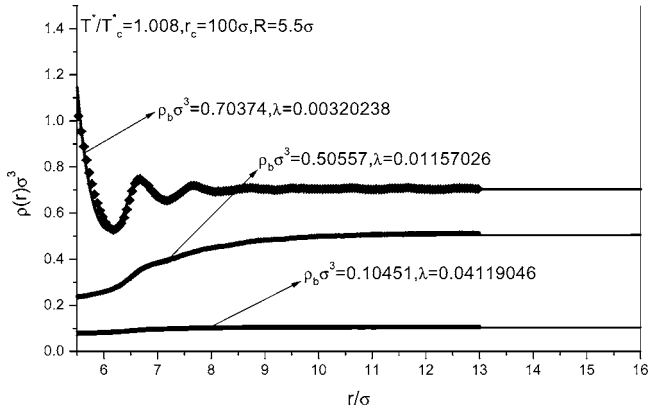

FIG. 9. Same as Fig. 7 but for $T^*/T_c^*=1.008$.

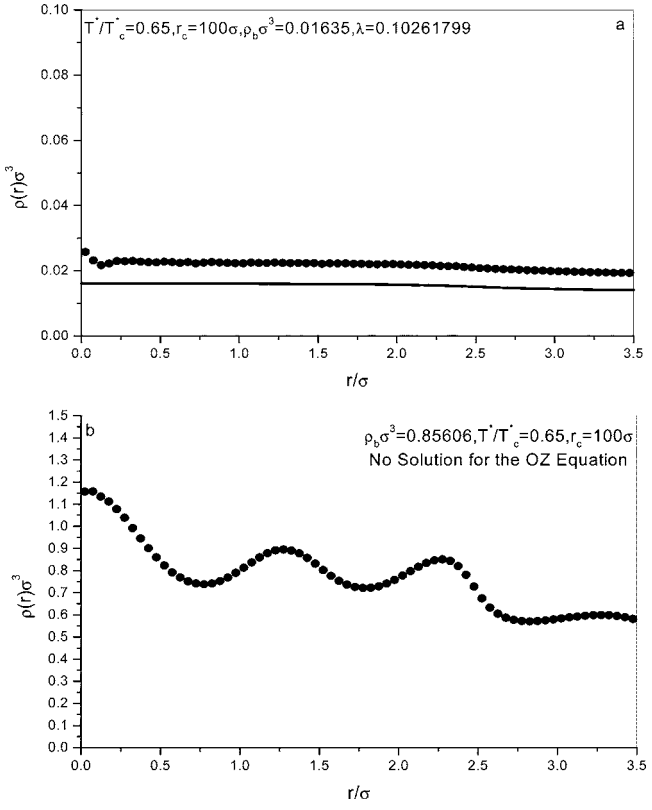

FIG. 10. The theoretical (lines) and simulation (symbols) results for the density profiles of the LJ fluid in a spherical cavity of an effective radius $R=3.5\sigma$ at the ratio between the actual and critical reduced temperature $T^*/T_c^*=0.65$ and at different values of the bulk reduced density.

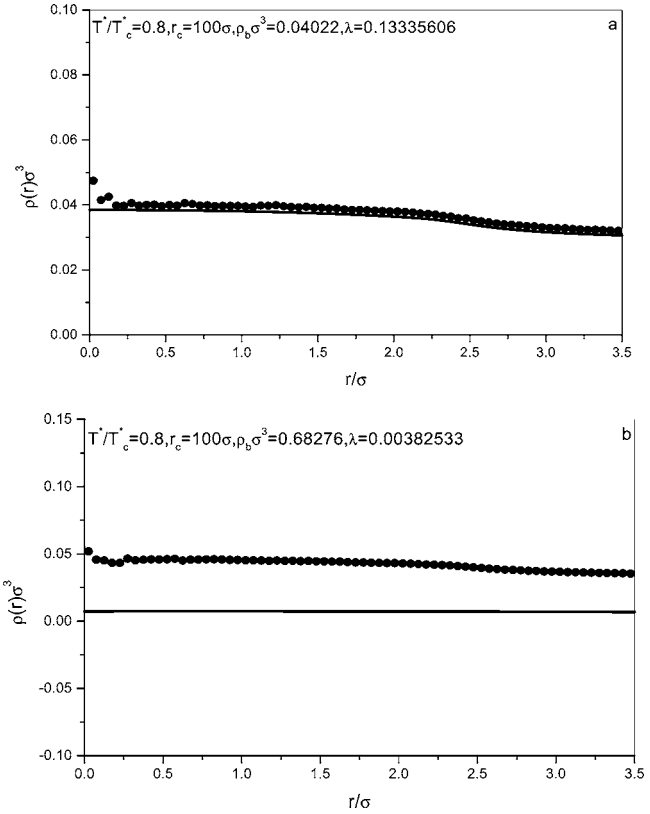

FIG. 11. Same as Fig. 10 but for $T^*/T_c^*=0.8$.

tured correctly. However, its performance can be excellent only in the case of high accuracy of the required bulk second order DCF and pressure of the bulk equilibrium fluid.

IV. SUMMARY

We have calculated the density profiles for the Lennard-Jones fluid in various confined systems from GCEMC simulations and from the density functional theory formalism. From a comparison between the theoretical predictions and the simulation data the following conclusions can be drawn. The third and second order perturbation DFT approach for the LJ fluid under the influence of external fields is structured correctly, the accuracy of the predictions for the density profiles being assured with an accurate bulk second order DCF as an input. This argument can be taken rigorously because we explored some "dangerous" regions of the phase diagram of the bulk LJ fluid. Two advantages are associated with the present perturbation DFT approach. The first is its computational simplicity, and the second its applicability to both supercritical and subcritical regimes. As the LJ pair potential comprises a highly repulsive soft core instead of a pure hard-core repulsion, its treatment by splitting the potential or direct correlation function into hard-core part and attractive tail part is somewhat puzzled regarding the question of how to determine the hard core diameter. In the present

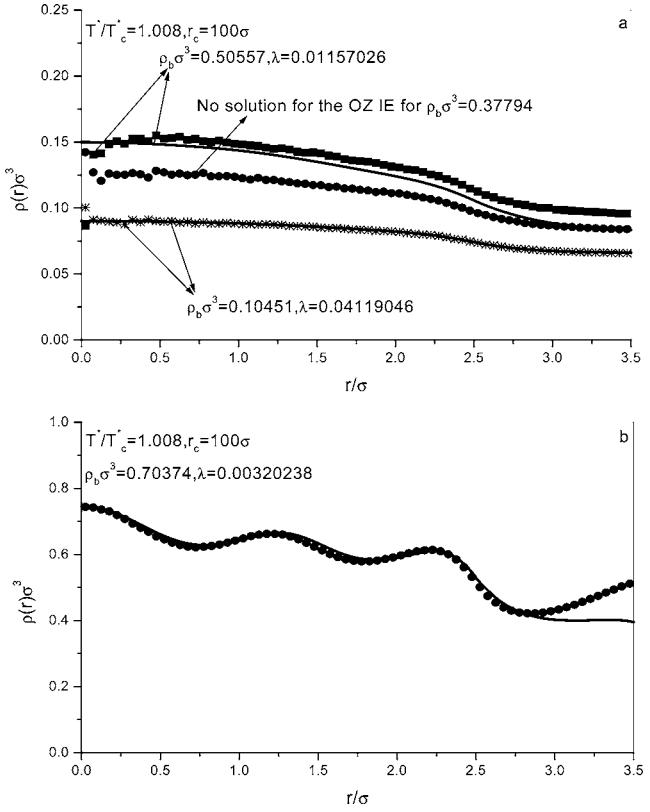

FIG. 12. Same as Fig. 10 but for $T^*/T_c^*=1.008$.

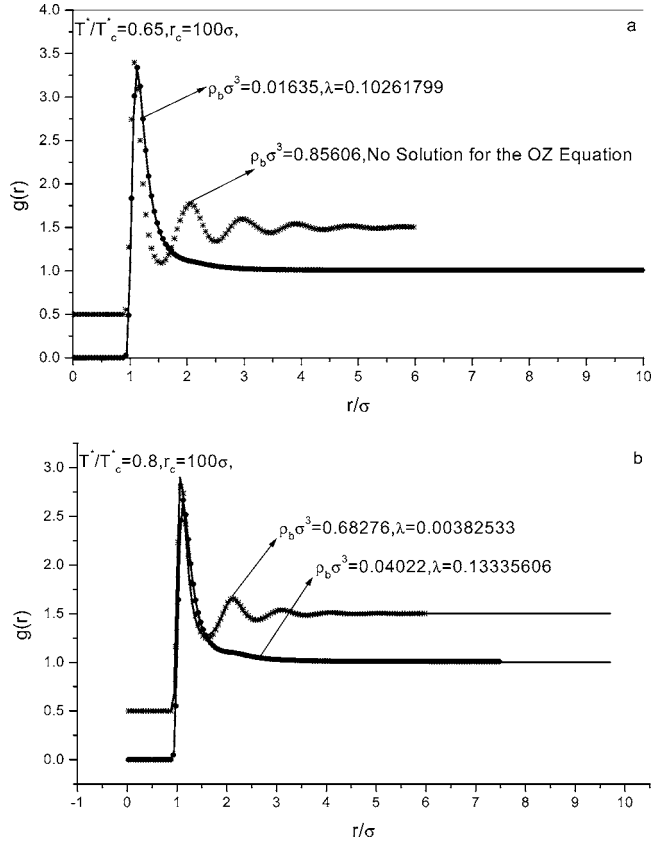

FIG. 13. The theoretical (lines) and simulation (symbols) results for the bulk radial distribution function of the LJ model fluid at two subcritical temperatures and at different densities. For the reason of clarity, the data corresponding to individual densities in each subfigure are shifted upwards by the factor 0.5.

perturbation DFT approach, the value of r_{cut} can simply be set to the LJ size parameter σ. This simplicity will become more obvious and important when we extend the present approach to fluid mixtures. When the coexistence bulk fluid is in thermodynamically stable state, then the solution of the Ornstein-Zernike integral equation for the bulk second order DCF, in principle, always exist. As in the present approach one needs only the bulk second order DCF of the coexistence bulk fluid as an input, it is, in principle, applicable to both the supercritical and subcritical temperatures. In practice, however, this is not always the case. As shown in the preceding chapter, there is no numerical solution to the OZ

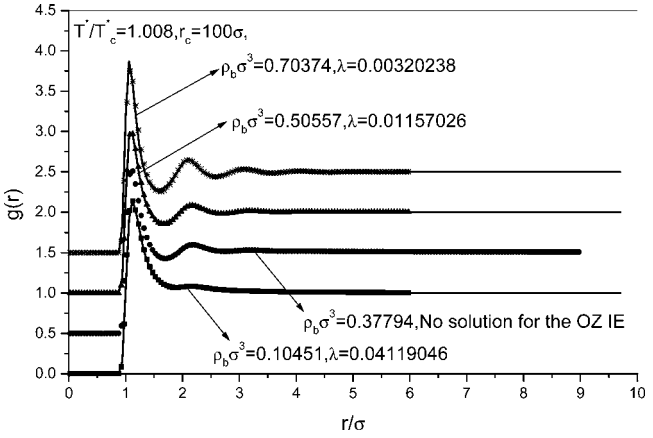

FIG. 14. The theoretical (lines) and simulation (symbols) results for the bulk radial distribution function of the LJ model fluid at a supercritical state and at different densities. For the reason of clarity, the data corresponding to individual densities in each subfigure are shifted upwards by different factors (0.5, 1,1.5, etc.).

equation for the two sets of parameters: (i) $\rho_b\sigma^3=0.377\,94$, $T^*/T_c^*=1.008$ (in the phase diagram, this supercritical state is located close to the critical point), and (ii) $\rho_b\sigma^3=0.85606$, $T^*/T_c^*=0.65$ (this subcritical state is located in the vicinity of the gas-liquid coexistence curve), though the simulation results indicate the thermodynamic stability of these states. This deficiency of the theory is caused by the approximation made in the bridge function. As many interesting phenomena occur at the conditions corresponding to the near-critical region and regions close to the gas-liquid coexistence curve, the problem of obtaining the bulk second order DCF for these "severe" conditions is of crucial importance and represents a challenging future theoretical work. For this reason, there is also additional motivation for an extension of the present study (focusing on a broad range of temperatures) to test the applicability of the present theoretical approach for a series of subcritical temperatures near the critical point (e.g., for T^*/T_c^* ranging between 0.95 and 0.99). We intend to report on this extension in a separate paper.

ACKNOWLEDGMENTS

A.J. acknowledges the support of the Slovenian Research Agency through the Grants Nos. P1-0201 and J1-6653. This project was supported also by the National Natural Science Foundation of China (Grant No. 20546004).

[1] S. Zhou, Phys. Rev. E **68**, 061201 (2003).
[2] S. Zhou and E. Ruckenstein, Phys. Rev. E **61**, 2704 (2000).
[3] S. Zhou and A. Jamnik, J. Chem. Phys. **122**, 064503 (2005).
[4] E. Waisman, Mol. Phys. **25**, 45 (1973); J. S. Hoye and G. Stell, *ibid.* **32**, 195 (1976).
[5] E. Diaz-Herrera, G. Ramirez-Santiago, and J. A. Moreno-Razo, Phys. Rev. E **68**, 061204 (2003); J. K. Brennan and W. Dong, *ibid.* **67**, 031503 (2003); C. Muguruma, Y. Okamoto, and M. Mikami, J. Chem. Phys. **120**, 7557 (2004); K. Maeda, W. Matsuoka, T. Fuse, K. Fukui, and S. Hirota, J. Mol. Liq. **102**, 1 (2003).
[6] E. Diaz-Herrera, J. A. Moreno-Razo, and G. Ramirez-Santiago, Phys. Rev. E **70**, 051601 (2004); V. G. Baidakov, G. G. Chernykh, and S. P. Protsenko, Chem. Phys. Lett. **321**, 315 (2000); J. J. Potoff and A. Z. Panagiotopoulos, J. Chem. Phys. **112**, 6411 (2000).
[7] K. Nishio, J. Koga, T. Yamaguchi, and F. Yonezawa, J. Non-Cryst. Solids **345**, 694 (2004); Phys. Rev. B **69**, 214201

(2004); A. Patrykiejew, L. Salamacha, and S. Sokolowski, J. Chem. Phys. **118**, 1891 (2003); D. Duque, J. C. Pamies, and L. F. Vega, *ibid.* **121**, 11395 (2004).

[8] D. Frenkel and B. Smit, *Understanding Molecular Simulation* (*Academic Press*, Boston, MA, 1996).

[9] J. J. Potoff and A. Z. Panagiotopoulos, J. Chem. Phys. **109**, 10914 (1998).

[10] S. Zhou, Commun. Theor. Phys. **40**, 721 (2003).

[11] L. Verlet, Mol. Phys. **41**, 183 (1980).

[12] N. Choudhury and S. K. Ghosh, J. Chem. Phys. **116**, 8517 (2002).

[13] J. M. Bomont and J. L. Bretonnet, Mol. Phys. **101**, 3249 (2003).

[14] L. L. Lee, J. Chem. Phys. **103**, 9388 (1995); S. Zhou and X. Zhang, Acta Physico-Chimica Sinica. 18, 699 (2002).

[15] D.-M. Duh and A. D. J. Haymet, J. Chem. Phys. **103**, 2625 (1995).

[16] J. K. Percus, in *The Equilibrium Theory of Classical Fluids*, edited by H. L. Frisch and A. L. Lebowitz (Benjamin, New York, 1964), p. 113.

[17] F. van Swol and J. R. Henderson, Phys. Rev. A **40**, 2567 (1989).